



## Multiresolution atomistic simulations of dynamic fracture in nanostructured ceramics and glasses

RAJIV K. KALIA<sup>1</sup>, AIICHIRO NAKANO<sup>1</sup>, PRIYA VASHISHTA<sup>1</sup>,  
CINDY L. ROUNTREE<sup>2</sup>, LAURENT VAN BRUTZEL<sup>3</sup> and SHUJI OGATA<sup>4</sup>

<sup>1</sup>Collaboratory for Advanced Computing and Simulations, University of Southern California, Los Angeles, CA 90089, U.S.A

<sup>2</sup>Department of Physics and Astronomy, Louisiana State University, Baton Rouge, LA 70803, U.S.A.

<sup>3</sup>CEA, Centre de la Valle du Rhone, Marcoule, B.P. 171, 30207 Bagnols Sur Ceze, France

<sup>4</sup>Graduate School of Engineering, Nagoya Institute of Technology, Nagoya 466-8555, Japan

**Abstract.** Multimillion atom molecular-dynamics (MD) simulations are performed to investigate dynamic fracture in glasses and nanostructured ceramics. Using multiresolution algorithms, simulations are carried out for up to 70 ps on massively parallel computers. MD results in amorphous silica (a-SiO<sub>2</sub>) reveal the formation of nanoscale cavities ahead of the crack tip. With an increase in applied strain, these cavities grow and coalesce and their coalescence with the advancing crack causes fracture in the system. Recent AFM studies of glasses confirm this behavior. The MD value for the critical stress intensity factor of a-SiO<sub>2</sub> is in good agreement with experiments. Molecular dynamics simulations are also performed for nanostructured silicon nitride (n-Si<sub>3</sub>N<sub>4</sub>). Structural correlations in n-Si<sub>3</sub>N<sub>4</sub> reveal that interfacial regions between nanoparticles are amorphous. Under an external strain, nanoscale cavities nucleate and grow in interfacial regions while the crack meanders through these regions. The fracture toughness of n-Si<sub>3</sub>N<sub>4</sub> is found to be six times larger than that of crystalline  $\alpha$ -Si<sub>3</sub>N<sub>4</sub>. We also investigate the morphology of fracture surfaces. MD results reveal that fracture surfaces of n-Si<sub>3</sub>N<sub>4</sub> are characterized by roughness exponents 0.58 below and 0.84 above a certain crossover length, which is of the order of the size of Si<sub>3</sub>N<sub>4</sub> nanoparticles. Experiments on a variety of materials reveal this behavior. The final set of simulations deals with the interaction of water with a crack in strained silicon. These simulations couple MD with a quantum-mechanical (QM) method based on the density functional theory (DFT) so that chemical processes are included. For stress intensity factor  $K = 0.4 \text{ MPa m}^{1/2}$ , we find that a decomposed water molecule becomes attached to dangling bonds at the crack or forms a Si-O-Si structure. At  $K = 0.5 \text{ MPa m}^{1/2}$ , water molecules decompose to oxidize Si or break Si-Si bonds.

**Key words:** Molecular dynamics; dynamic fracture; nanostructured ceramics; glasses.

### 1. Introduction

Recent advances in massively parallel computations coupled with the development of accurate interatomic interactions have made it possible to apply atomistic simulations to reliably investigate dynamic fracture in a variety of materials (Vashishta and Nakano, 1999). In this paper we describe some of our recent research on atomistic simulations of nanostructured ceramics and glasses. Section 2 contains a brief description of the parallel molecular-dynamics (MD) approach and interatomic potentials used in fracture simulations. In Section 3, we discuss the results of multimillion atom MD simulations of crack propagation in amorphous silica (a-SiO<sub>2</sub>) and nanostructured silicon nitride (n-Si<sub>3</sub>N<sub>4</sub>). Scaling properties of fracture surfaces and comparison with experimental results are presented in Section 4. In Section 5, we describe our recent multiscale simulation study of the interaction between water molecules and a crack

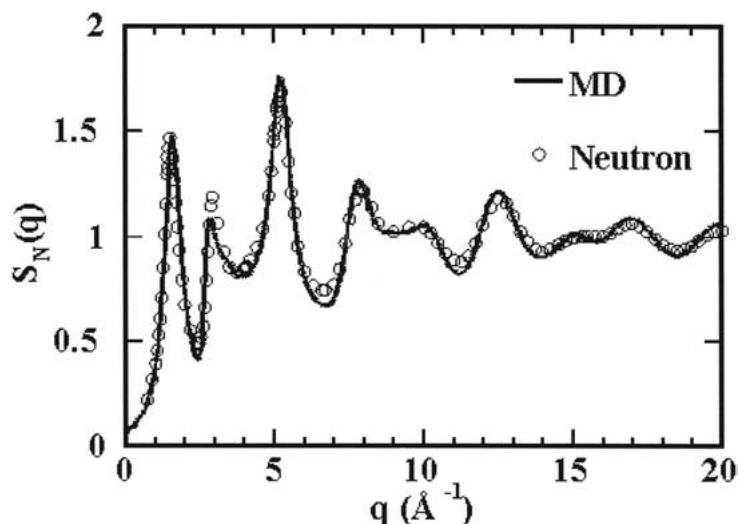


Figure 1. Comparison between neutron scattering and MD results for the static structure factor of amorphous silica.

in silicon. The multiscale approach combines classical MD with a quantum-mechanical (QM) scheme based on the density functional theory (DFT). The latter explicitly includes chemical processes.

## 2. Molecular dynamics simulations on massively parallel machines

Most of the simulations reported here employ the classical MD approach, which involves numerical integration of Newton's equations for atoms (Allen and Tildesley, 1989). The numerical solution yields atomic positions and velocities at discrete intervals of time. From atomic trajectories, thermodynamic, structural, dynamical, and mechanical properties can be calculated.

The essential input to an MD simulation is a reliable interatomic potential. In recent years, we have developed accurate interatomic interactions for  $\text{SiO}_2$ ,  $\text{Si}_3\text{N}_4$ , and a variety of other ceramic and semiconducting materials (Vashishta et al., 1990). Silica and silicon nitride are ionic as well as covalent in nature. Both effects are included through a combination of two-body and three-body interactions. The two-body potential consists of steric repulsion, screened Coulomb interaction due to charge transfer among atoms, and charge-dipole interaction. Covalent effects are included through three-body bond-bending and bond-stretching terms.

Interaction potentials are validated by comparing MD results for various material properties with corresponding experimental measurements or first-principles DFT calculations. As an example, we show in Figure 1 the MD and neutron scattering static structure factors for  $\alpha\text{-SiO}_2$  (Nakano et al., 1994). The comparison shows how well the MD simulation describes short-range correlations (large wave vectors) and medium-range order (the first sharp diffraction peak) in the system. We also find the calculated elastic moduli of  $\alpha\text{-SiO}_2$  are in good agreement with experimental results. Figure 2 shows a comparison between MD and experimental results for phonon density of states of crystalline  $\alpha\text{-Si}_3\text{N}_4$  (Loong et al., 1995).

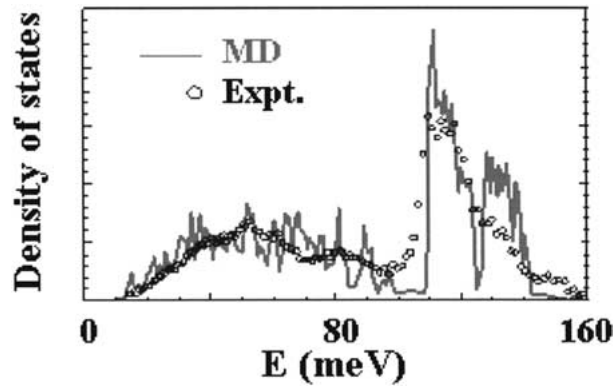


Figure 2. Comparison between the MD calculation and inelastic neutron scattering measurements of phonon density of states of crystalline  $\alpha$ -Si<sub>3</sub>N<sub>4</sub>.

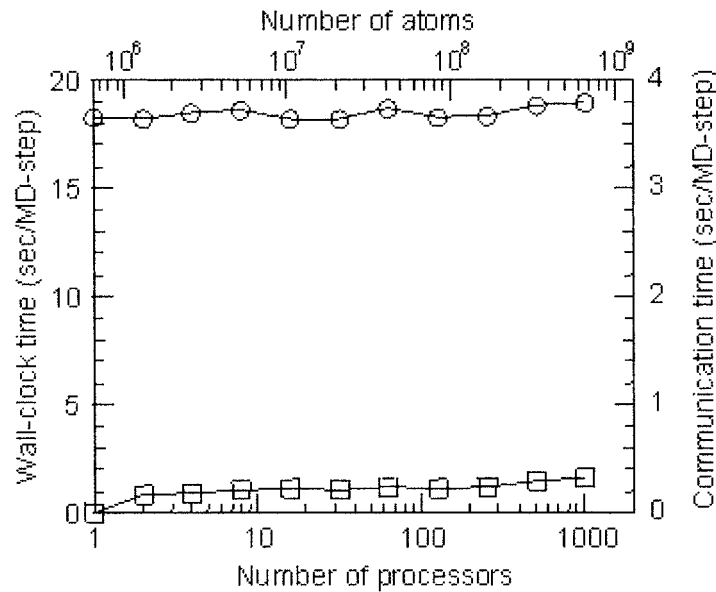
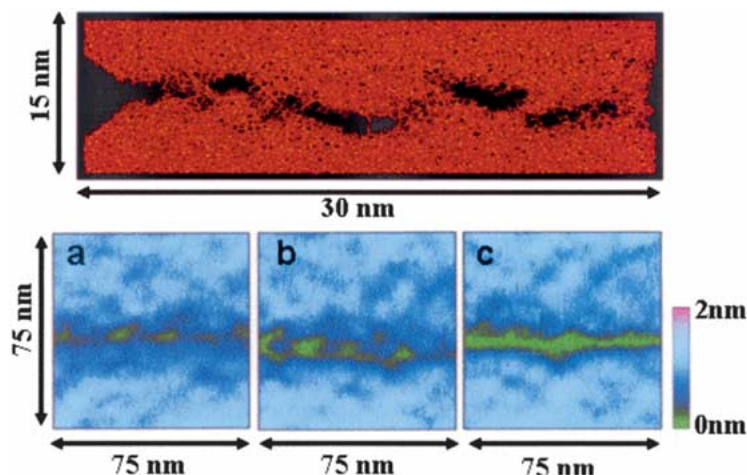


Figure 3. MD benchmark for a-SiO<sub>2</sub> on a Cray T3E parallel computer. Circles and squares show scaling of the wall-clock time, the time difference between the start and end of the program, and interprocessor communication time per MD time step, respectively, with the number of atoms,  $N$ , in the system.  $N$  is increased linearly with the number of processors,  $p$ . The wall-clock time remains constant over three orders-of-magnitude increase in  $N$  (from 10<sup>6</sup> to 10<sup>9</sup> atoms), which implies linear scaling of the wall-clock time with the system size.

The calculated elastic moduli of  $\alpha$ -Si<sub>3</sub>N<sub>4</sub> and the static structure factor of amorphous Si<sub>3</sub>N<sub>4</sub> are also in good agreement with corresponding measurements (Loong et al., 1995).

Molecular dynamics calculations of fracture in a-SiO<sub>2</sub> and Si<sub>3</sub>N<sub>4</sub> are computationally challenging because they require sufficiently large systems with compute-intensive interatomic forces. We have designed algorithms that reduce the execution time significantly and map very well onto parallel computers. In addition, algorithms have been designed to make the simulation scheme scalable and portable on parallel machines. One of these algorithms – an adaptive load balancer for non-homogeneous systems (Nakano and Campbell, 1997) – is particularly important to atomistic simulations of crack propagation. This load-balancing algorithm performs uniform domain decomposition of the system in curvilinear space to



*Figure 4.* (Top) Snapshot of atoms ( $t = 55$  ps) in a MD simulation of fracture in a-SiO<sub>2</sub> at room temperature shows nanometer scale cavities (black) in front of the crack, cavity coalescence, and merging of cavities with the advancing crack. (Bottom) AFM picture of a stress corrosion crack (i.e. sub-critical crack growth where the corrosion by the water contained in the atmosphere assists the crack propagation) in an aluminosilicate glass at room temperature reveals nanometric cavities (green) ahead of the crack. With the FRASTA (Fracture-surface Topography Analysis) method, it is shown that the voids contribute to the final fracture and are actually damage cavities. Recently, the group has observed the same fracture mechanism in silica glass (E. Bouchaud, private communications).

balance the computational ‘load’ and minimize communication among parallel processors. Figure 3 shows the performance of our parallel MD code on a 1024-processor Cray T3E machine. The wall-clock time (the time difference between the start and end of the program) remains nearly the same over three orders-of-magnitude increase in the system size. Since the system size is increased linearly with the number of processors, these performance tests imply that MD algorithms scale linearly with the number of atoms in the system. Figure 3 also shows that interprocessor communication time is a small fraction of the wall-clock time. We have also designed a scalable I/O data-compression algorithm for post-simulation analysis (Sharma et al., 2002), which affords real-time immersive visualization of very large systems (up to a billion atoms).

### 3. Crack propagation in amorphous SiO<sub>2</sub> and nanostructured Si<sub>3</sub>N<sub>4</sub>

Amorphous silica (a-SiO<sub>2</sub>) was obtained by heating  $\beta$ -cristobalite to 3200 K and then quenching the molten system to room temperature. As shown in Figure 1, short-range spatial correlations and medium-range order in the computer-generated system are in good agreement with neutron scattering measurements. The calculated bond angle distribution, Si-O-Si, also compares very well with NMR measurements (Pettifer et al., 1988).

The amorphous system was notched and a uniaxial strain was applied to atoms within 7.5 Å (cut-off in the potential) from the outermost layers. Figure 4 shows that crack propagation is accompanied by nucleation and growth of nanometer scale cavities ahead of the crack tip. Cavities coalesce and merge with the advancing crack to ultimately cause failure. Recent experimental work of Bouchaud and coworkers (Célarié et al., 2003), involving an AFM study of fracture in a aluminosilicate glass, reveals nanocavitation and coalescence of cavities with

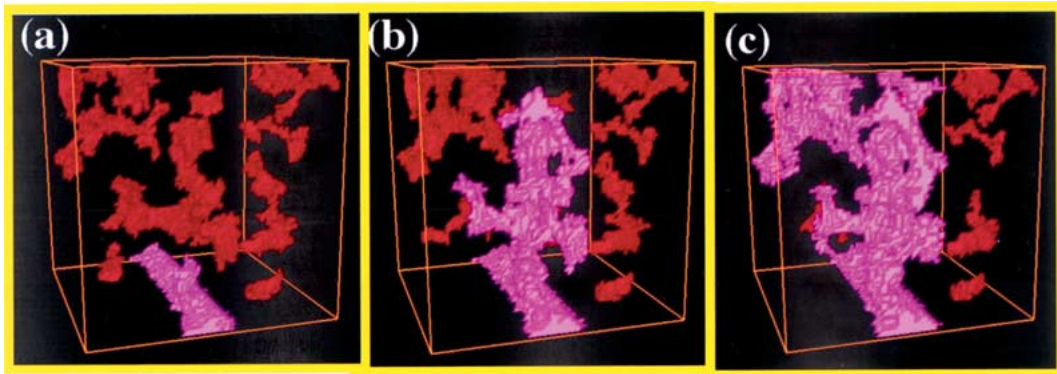


Figure 5. MD simulations of dynamic fracture in  $n\text{-Si}_3\text{N}_4$  at room temperature. Snapshots show the crack front (magenta) and the cavities (red) in  $n\text{-Si}_3\text{N}_4$  at 10 ps after applied strains of 5% (a), 11% (b), and 14% (c) were reached (Kalia et al., 1997).

the crack to be the mechanism of fracture. Our calculation of the critical stress intensity factor,  $K_{IC}$ , in  $\alpha\text{-Si-O}_2$  is  $1 \text{ MPa m}^{1/2}$  and the experimental values range between  $0.8 \text{ MPa m}^{1/2}$  and  $1.2 \text{ MPa m}^{1/2}$  (Van Brutzel et al., 2001).

Turning to nanostructured silicon nitride ( $n\text{-Si}_3\text{N}_4$ ), we first remove a spherical nanoparticle of diameter 6 nm from crystalline  $\alpha\text{-Si}_3\text{N}_4$ . The nanoparticle is thermalized at room temperature and then 108 different configurations of the nanoparticle are placed randomly in a cubic MD box (the system contains approximately  $10^6$  atoms.) The initial configuration is heated to 2000 K and subsequently sintered under hydrostatic pressures of 5, 10, and 15 GPa. The final sintered system (at 15 GPa) is cooled down and thermalized at room temperature. Subsequently, the pressure is reduced to 10 GPa, 5 GPa, and 0 GPa. In each instance, the system is relaxed for thousands of time steps. The final  $n\text{-Si}_3\text{N}_4$  configuration is consolidated to 92% of the density of crystalline  $\alpha\text{-Si}_3\text{N}_4$ .

MD calculations of Si-Si, Si-N, and N-N pair-distribution functions and Si-N-Si and N-Si-N bond-angle distributions reveal that interior regions of nanoparticles remain crystalline whereas interfacial regions between nanoparticles are akin to amorphous  $\text{Si}_3\text{N}_4$  (Kalia et al., 1997a). This was confirmed by MD simulations of amorphous  $\text{Si}_3\text{N}_4$  of the same mass density as the average mass density of interparticle regions in  $n\text{-Si}_3\text{N}_4$ . Partial pair-distribution functions and bond-angle distributions for the two systems are similar. As we shall see momentarily, the amorphous structure of interparticle regions play a key role in crack propagation in  $n\text{-Si}_3\text{N}_4$ .

In MD simulations of dynamic fracture in  $n\text{-Si}_3\text{N}_4$ , the sintered system at room temperature is notched and subjected to an external strain (Kalia et al., 1997b). Figure 5(a) is a snapshot of the system at 10 ps after the strain reaches 5%. (To highlight cavities and cracks in the system, atoms are not shown in the figure.) In addition to the notch (magenta), we observe nanoscale cavities in amorphous interparticle regions. As the strain is increased, the notch advances and cavities grow and coalesce among themselves and also with the advancing crack; see Figure 5(b). The crack front meanders through amorphous interparticle regions; see Figure 5(c). Nanoscale cavitation, crack meandering, and crack branching render  $n\text{-Si}_3\text{N}_4$  much tougher than  $\alpha\text{-Si}_3\text{N}_4$  crystal, which undergoes cleavage fracture. Fracture toughness of  $n\text{-Si}_3\text{N}_4$  is estimated to be 6 times larger than that of the crystal.

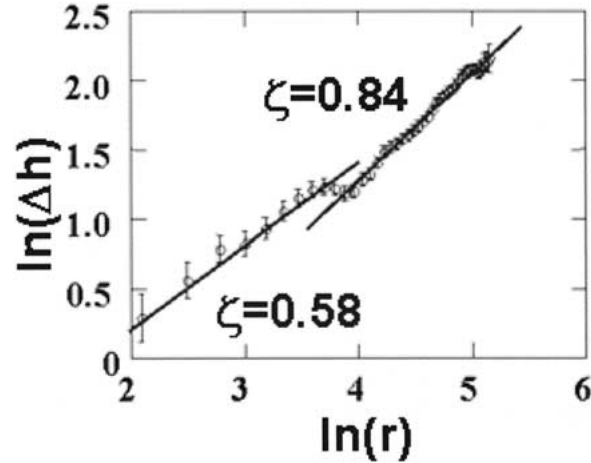


Figure 6. Height-height correlation function for fracture surfaces in  $n\text{-Si}_3\text{N}_4$ . The MD results show that the roughness exponents are 0.58 and 0.84 below and above a certain cross-over length, respectively. The cross-over length is close to the nanoparticle size.

We have also investigated crack propagation in amorphous nanostructured silica ( $n\text{-SiO}_2$ ). The system was generated by removing a spherical nanoparticle of diameter 8 nm from the bulk  $a\text{-SiO}_2$  system mentioned before. After thermalizing it at room temperature, 100 different configurations of the nanoparticle were placed randomly in a cubic box. Periodic boundary conditions were applied and the system was sintered at 1000 K under hydrostatic pressure of 16 GPa. Subsequently, the system was cooled down to room temperature and thermalized both before and after removing the pressure.

MD simulations of fracture in  $n\text{-SiO}_2$  reveal that the crack propagates through interparticle regions. At small values of the applied strain, these regions have a few isolated nanocavities. As the applied strain is increased, we observe: (a) the pre-crack advances mostly through interfacial regions; (b) nanocavities grow and coalesce; and (c) new nanocavities form ahead of the crack in interparticle regions. The crack meanders through nanoparticle boundaries, coalescing with nanocavities in its path, until the system completely fractures.

#### 4. Scaling properties of fracture surfaces

We have examined the morphology of fracture surfaces in  $n\text{-Si}_3\text{N}_4$  and have found scaling behavior akin to that observed experimentally in a variety of other materials. Fracture surfaces are self-affine objects with the height-height correlation function varying as:

$$\Delta h(r) = \langle (x(z+r) - x(z))^2 \rangle_z^{1/2} \propto r^\zeta, \quad (1)$$

where  $x$  is the height of the fracture profile normal to the plane of crack propagation and  $\langle \dots \rangle_z$  implies an average over  $z$ . Figure 6 shows our MD results for fracture surfaces in  $n\text{-Si}_3\text{N}_4$ . The log-log plot of  $\Delta h$  versus  $r$  reveals two distinct power-law regimes with exponents  $\zeta = 0.58$  and  $0.84$  below and above a cross-over length,  $\xi_c$ , respectively. The smaller exponent (0.58) is found to be due to intra-cavity correlations while the larger one (0.84) results from inter-cavity correlations and crack-cavity coalescence. The cross-over length,  $\xi_c$ , is close to the size of the nanoparticle.

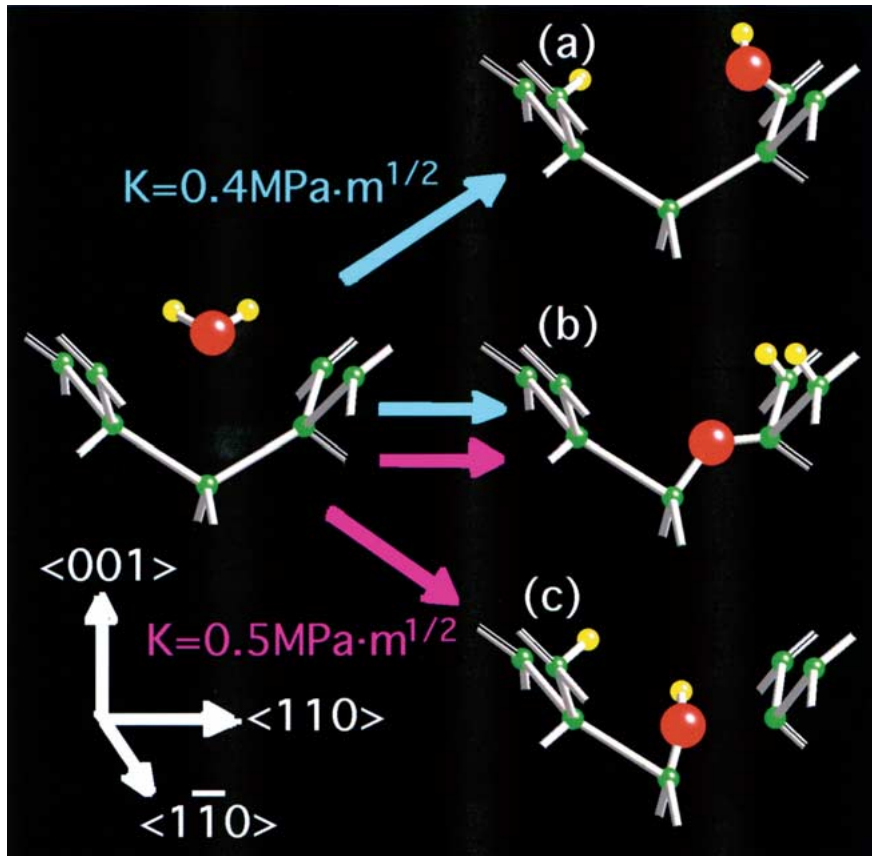


Figure 7. Interaction of water with a crack in silicon. Si atoms are green, oxygens are red, and hydrogens are yellow. Blue and magenta arrows indicate the behavior at stress intensity factors  $K = 0.4 \text{ MPa m}^{1/2}$  and  $0.5 \text{ MPa m}^{1/2}$ , respectively.

Fracture experiments on various metals, alloys, ceramics, and glasses reveal similar scaling behavior (Daguier et al., 1996, 1997). The experimental value of the lower exponent is around 0.5 while the larger exponent is always close to 0.8, independent of the material or its microstructure. The cross-over length  $\xi_c$  is, however, a material characteristic which decreases with an increase in the crack velocity.

## 5. Multiscale simulations of water-crack interaction in silicon

Recently, we performed the first hybrid quantum mechanical /classical MD simulation study of the effect of water on crack initiation in silicon (Ogata et al., submitted). The simulation involves a crystalline Si slab with  $x$ ,  $y$ , and  $z$  axes parallel to  $\langle 1\bar{1}0 \rangle$ ,  $\langle 110 \rangle$ , and  $\langle 001 \rangle$  directions, respectively. From the center of the slab, half of the atomic layer parallel to  $\langle 110 \rangle$  is removed to mimic a straight-edged crack along the  $\langle 1\bar{1}0 \rangle$  direction. Periodic boundary conditions along  $x$  and  $y$  and free boundary condition along  $z$  are imposed. The system is stretched uniformly along  $x$  and temperature is kept at OK by scaling atomic velocities.

The multiscale approach involves a quantum mechanical (QM) description of a cluster of atoms around the notch while the rest of the atoms are treated by MD using the Stillinger-

Weber potential for Si (Stillinger and Weber, 1985). The total Hamiltonian of the hybrid QM/MD system is,

$$H = H_{MD} + \sum_{cluster} E_{QM}^{cluster}(\{\vec{r}_{QM}\}, \{\vec{r}_{QM}\}) - E_{MD}^{cluster}(\{\vec{r}_{QM}\}, \{\vec{r}_{HS}\}), \quad (2)$$

where the first term is the potential energy of the entire system calculated with the classical MD approach and the second and third terms are the QM and MD energies of the atomic cluster in the notch region, respectively. In Equation (2)  $\{\vec{r}_{QM}\}$  and  $\{\vec{r}_{HS}\}$  denote the positions of QM and ‘handshake’ atoms, respectively. The latter are classical atoms bonded to QM atoms. In the quantum calculation for the atomic cluster, each quantum particle bonded to a ‘handshake’ atom is terminated by a hydrogen atom. A scaled position method with  $\{\vec{r}_{QM}\}$  and  $\{\vec{r}_{HS}\}$  as input is employed to determine the positions of termination hydrogen atoms (Ogata et al., 2001).

The calculation for the QM cluster with termination H atoms is performed within the framework of the density functional theory (DFT). We solve Kohn-Sham equations for valence electrons:

$$\left[ -\frac{\Delta}{2} + V_{Hartree}(\vec{x}) + V_{ion}(\vec{x}) + V_{xc}(\rho(\vec{x})) \right] \psi_i = \varepsilon_i \psi_i, \quad (3)$$

where  $\psi_i$  is a Kohn-Sham wave function for electrons,  $V_{Hartree}$  is the Hartree potential,  $V_{ion}$  is the pseudopotential for valence electrons, and  $V_{xc}$  is the electronic exchange-correlation potential.  $V_{Hartree}$  is obtained from the solution of,

$$\Delta V_{Hartree}(\vec{x}) = -4\pi\rho(\vec{x}), \quad (4)$$

where

$$\rho(x) = 2 \sum_{i=1}^{occupied} |\psi_i(\vec{x})|^2. \quad (5)$$

Equations (3)–(5) are solved numerically on a real-space three-dimensional grid (Shimojo et al., 2001).

The hybrid QM/MD simulations involve a cluster of 108 Si atoms and 120 termination H atoms. Three H<sub>2</sub>O molecules with random orientations and zero velocities are inserted in different regions of the crack. (This process was repeated for different initial random orientations of the H<sub>2</sub>O molecules and similar results were found.) Simulations are performed at stress-intensity factors  $K = 0.4 \text{ MPa m}^{1/2}$  and  $0.5 \text{ MPa m}^{1/2}$ . At  $K = 0.4 \text{ MPa m}^{1/2}$ , two of the three water molecules dissociate into H and OH and attach to Si dangling bonds at the crack. The third molecule breaks up into 2H and an O with the H atoms attached to dangling Si bonds and the O atom bonded to two Si atoms; see Figure 7. At  $K = 0.5 \text{ MPa m}^{1/2}$ , two of the three H<sub>2</sub>O molecules dissociate into 2H and an O with H atoms attached to dangling Si atoms and the O bonded to two Si atoms in the crack. The third molecule dissociates into an H and OH with the H adhering to a dangling Si bond while the OH breaks a Si-Si bond at the crack front (see Figure 7). Currently, a number of calculations are underway to investigate the interaction of H<sub>2</sub>O with other cracked Si surfaces that are partially saturated with H atoms.

## References

Allen, M.P. and Tildesley, D.J. (1989). *Computer Simulation of Liquids* Oxford University Press. Reprint Edition (August 1989).

- Célerié, F., Prades, S., Bonemy, D., Ferrero, L., Bouchaud, E., Guillot, C., and Marlière, C. (2003) *Physical Review Letters* **90**, 075504-1-075504-4.
- Daguier, P., Bouchaud, E., Lapasset, G. (1996). *Journal de Physique IV* **6**, 483–490.
- Daguier, P., Nghiem, B., Bouchaud, E. and Creuzet, F. (1997). *Physical Review Letters* **78**, 1062–1065.
- Kalia, R.K., Nakano, A., Tsuruta, K. and Vashishta, P. (1997). *Physical Review Letters* **78**, 689–692.
- Kalia, R.K., Nakano, A., Tsuruta, K. and Vashishta, P. (1997). *Physical Review Letters* **78**, 2144–2147.
- Loong, C.K., Vashishta, P., Kalia, R.K. and Ebbsjö, I. (1995). *Europhysics Letters* **31**, 201–206.
- Nakano, A. and Campbell, T. (1997). *Parallel Computing* **23**, 1461–1478.
- Nakano, A., Bi, L., Kalia, R.K. and Vashishta, P. (1994). *Physical Review B* **49**, 9441–9452.
- Ogata, S., Shimojo, F., Nakano, A., Kalia, R.K. and Vashishta, P. *Journal of Applied Physics*, submitted.
- Ogata, S., Lidorikis, E., Shimojo, F., Nakano, A., Vashishta, P. and Kalia, R.K. (2001). *Computer Physics Communications* **138**, 143–154.
- Pettifer, R.F., Dupree, R., Farnan, I. and Sternberg, U. (1988). *Journal of Non-Crystalline Solids* **106**, 408–412.
- Sharma, A., Miller, P., Liu, X., Nakano, A., Kalia, R.K., Vashishta, P., Zhao, W., Campbell, T.J. and Haas, A. (2002). in *Proceedings of IEEE Virtual Reality 2002 Conference* (IEEE Computer Society, Los Alamitos, CA, 2002) pp. 217–223.
- Shimojo, F., Kalia, R.K., Nakano, A. and Vashishta, P. (2001). *Computer Physics Communications* **140**, 303–314.
- Stillinger, F.H. and Weber, T.A. (1985). *Physics Review B* **31**, 5262–5271.
- Van Brutzel, L., Rountree, C.L., Kalia, R.K., Nakano, A. and Vashishta, P. (2001). *MRS Proceedings* **703**, 3.9.1–3.9.6.
- Vashishta, P. and Nakano, A. (1999). *Computing in Science & Engineering* **1**, 20–23.
- Vashishta, P., Kalia, R.K., Rino, J.P. and Ebbsjö, I. (1990). *Physical Review B* **41**, 12197–12209.